MIT Libraries | DSpace@MIT

MIT Open Access Articles

Out-of-plane neural microelectrode arrays fabrication using conventional blade dicing

Massachusetts Institute of Technology

CrossMark

ORIGINAL ARTICLE

Out-of-plane neural microelectrode arrays fabrication using conventional blade dicing

S. B. Goncalves[1] (ID) · M. J. Oliveira[2] · A. C. Peixoto[2] · A. F. Silva[1] · J. H. Correia[2]

Abstract This paper describes an optimized out-of-plane fabrication method for neural 3D high-aspect-ratio microelectrode array (MEA) based on a dicing technology platform (a standard procedure in semiconductor industry). The proposed MEA fabrication required important modifications in the dicing process. Since electrodes length reaches up to 4 mm, the main hindrance was the 2 mm cutting depth limit allowed for dicing machines with regular blades. This new procedure consisted on modifying Z-axis calibration, so cuts as deep as the exposure of blades were possible. The employment of proper blades for each fabrication step was also mandatory. Thin and high-exposure blades were used for deep cuts in silicon wafers, and V-shaped blades were employed to produce sharpened tips on the electrodes. Moreover, parameters as very low-cut speeds were essential to avoid wafer chipping and microcracks. Results showed high-precision and high-quality cuts in all steps of the 3D

MEA fabrication, without unnecessary additional steps of etching post-processing. The optimized fabrication process was successfully demonstrated with a 3D neural probe array comprising 36 individually addressable electrodes.

Keywords Dicing saw · Diamond blade · Neural microelectrode array · Silicon wafer

1 Introduction

A wide variety of fabrication methods have been used for the production of neural probes. However, most of fabrication approaches for these kind of devices rely on planar microfabricated 2D MEA [1, 2] or 3D structures assembled by layers of 2D arrays [3, 4]. 2D arrays miss three-dimensional neural information, recording in a single plane of the brain, while 3D arrays assembled by 2D parts require complex assembly steps and vertical interconnection [3]. 3D probes designs had mostly employed in-plane fabrication methods like dry- and wet-etching processes [5–7].

Out-of-plane fabrication techniques such as micro-wire electrical discharge machining [8], self-assembled probes using heat treatment [5], and magnetic processes [9] have also been used to produce 3D MEA. Yet, these techniques are not standard micromachining technology and limit the number of shafts in the array. A different approach to fabricate out-of-plane 3D probes was introduced by Campbell et al. [10]. This technology relies on silicon wafer micromachining using blade dicing technique, which resulted in a widely used tool in neuroscience, the Utah Electrode Array (UEA). Using the same technique, we also have previously presented an approach to fabricate 3D MEA using both aluminum [11] and silicon [12] as the bulk materials.

✉ S. B. Goncalves
  sgoncalves@dei.uminho.pt

  M. J. Oliveira
  mariajlcoliveira@gmail.com

  A. C. Peixoto
  alexbr82@gmail.com

  A. F. Silva
  asilva@dei.uminho.pt

  J. H. Correia
  higino.correia@dei.uminho.pt

[1] MIT Portugal Program, School of Engineering, University of Minho, Guimaraes 4800-058, Portugal

[2] Department of Industrial Electronics, University of Minho, Guimaraes 4800-058, Portugal

Blade dicing has been the most widely used process in the separation of silicon wafers into individual chips/devices both in semiconductor and micro-electro-mechanical systems (MEMS) technologies [13–15]. Since blade dicing is a purely mechanical process, its employment can produce undesirable mechanical vibrations, stress, and localized defects in the wafer [16]. Therefore, fabrication of extremely challenging devices such as MEMS and 3D devices push mechanical dicing process to its limits. Manufacturing of such different designs and fragile devices represents a challenge to the dicing technology and might require modifications to the dicing process. In fact, as the component parts size decreases and the cutting parameters becomes smaller, the whole aspect of machining can suffer changes [17].

There are some critical factors that influence cutting processes quality, such as blade characteristics (diamond grit size, exposure, and thickness), feed speed, spindle speed, cut depth, and saw street pattern [18]. These parameters must change depending on the desired application. Particularly, 3D arrays fabrication relying entirely on blade dicing requires high precision cuts on the bulk material. Cuts quality must ensure low substrate chipping and avoid microcracks [19]. To obtain high aspect-ratio and density of electrodes, thin deep grooves on thick silicon wafers must also be accomplished.

In this paper, it is used an automatic dicing saw machine to manufacture the 3D MEA for neural applications. Processes for overcoming the challenges in MEA fabrication process using blade dicing technology will be discussed and explored.

2 Fabrication

2.1 Dicing machine

All cuts are carried out by a high precision Disco DAD 2H/6T dicing saw (Fig. 1a). Mechanical dicing process uses a dicing equipment to fully or partially cut through wafers. Usually, a wafer is placed into a mounting/dicing tape, which has an adhesive layer on top, so it can be safely attach to the vacuum chuck during dicing process, and it can be easily detached in the end. The mounting tape is held in the chuck with the aid of suction. The chuck moves at a specific and constant feed rate passing through the dicing blade in X and Y directions for device cutting. The feed speed or cut speed determines how fast the sample is fed against the saw blade.

The cutting tool is called the dicing blade and is mounted in the spindle of the dicing equipment (Fig. 1b, c). Dicing blades have synthetic diamond particles held in place by a metal support (flange) and exhibit diamond particles in one

or both of their sides. The dicing wheel (spindle) spins at a constant rotational velocity, typically between 30,000 and 50,000 rpm. All experiments were carried out at 30,000-rpm spindle speed.

As a preparation step for dicing, calibration of the blade height (Z-axis level), measured from a reference level (Z=0), must be performed. This is accomplished by promoting electrical contact between the blade edge and the surface of the chuck. Z-axis calibration (determines when Z=0) sets the maximum cut depth of the blade. The double lens microscope is equipped with two 15 W lamps for easy alignment between sample and blade.

Cutting processes create substantial amount of heat within the blade. Thus, a proper wheel cooling (deionized water jet) is used in order to keep the blade at low temperature and ensure that the wheel does not loose its structural integrity. Also, as deionized water is used the ions are removed from the water, ensuring samples free of ionic contamination. After cutting, a nitrogen spray gun can be used to dry off samples and chuck.

2.2 Dicing challenges

In order to accomplish the design of some challenging devices like 3D probes, carefully selection of the cut parameters is mandatory. Indeed, the optimization of its parameters can broaden the application of most machining processes, allowing the production of various complex parts or devices [20].

High density of electrodes is a feature that 3D arrays aspire. To accomplish this, grooves areas have to be minimized, i.e., the space between elements reserved for the separation cut has to be kept as small as possible. Then, ultra-thin blades should be used in the dicing process. While electrodes density is an important feature of 3D arrays, so it is high aspect-ratio electrodes, which allows to reach deeper neural structures. Therefore, a trade-off between groove saw width and cuts depth has to be made.

Other significant fabrication challenge consists on dicing different materials in the array. Depending on the material, it can exhibit different behavior when diced. Typically, semiconductors like silicon, ceramics, and glasses present brittle mode cutting, which frequently induce microcracks within the material and chipping occurs at the edges [21, 22]. The minimization of these effects has been a priority fabrication issue.

Moreover, the choice of a sui blade is crucial. Blade exposure (difference between blade and flange radius—see Fig. 1c) plays an important role to achieve deep cuts, since it determines the maximum depth of the cut. Blades with high exposure have to be strong enough to withstand dicing on thick wafers. This phenomena hinders the employment
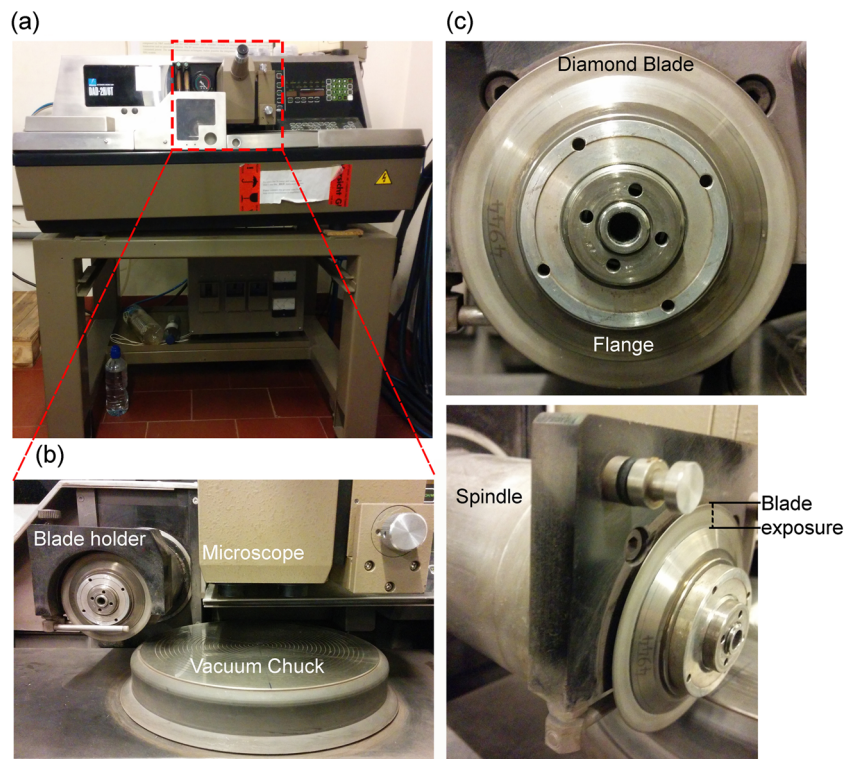
of ultra-thin blades and decreases the overall electrodes density.

3D arrays comprising 4 mm-deep electrodes are created, and yet dicing equipment just allows cuts up to 2 mm in height. Therefore, some modifications must be made in the way dicing machine performs Z-axis calibration in order to cut samples above its 2 mm limit. By placing an aluminum spacer between blade and chuck, it is possible to cut up to 4 mm high. This spacer is manually introduced just for the set-up of the machine and is removed afterwards. This method is illustrated in Fig. 2.

Cutting programs for dicing silicon wafers rely mainly on three variables: speed of cut (feed speed), Y-axis step, which determines the distance between two cuts, and Z-axis level, which determines the depth of cut. The cut program is performed automatically, altering previous mentioned parameters depending on the fabrication step. After completion of each sequence of steps, the program repeats itself until the entire wafer is diced.

2.3 Silicon MEA fabrication

In this section, we discuss how silicon wafers are micromachined to manufacture a 3D MEA design. The proposed MEA consists of 36 sharp electrode probes with three different electrode lengths: 3, 3.5, and 4 mm. Its structure is divided into three regions: a support base region, the electrode body (shaft), and a piercing region (sharp tip) that is simultaneously the recording/stimulation region (Fig. 3). Electrodes tips are placed 600 μm from each other.

Fig. 2 **a** Standard and **b** modified Z-axis calibration during set-up of the dicing machine. t represents the spacer's thickness, which depends on the desired depth of the cut
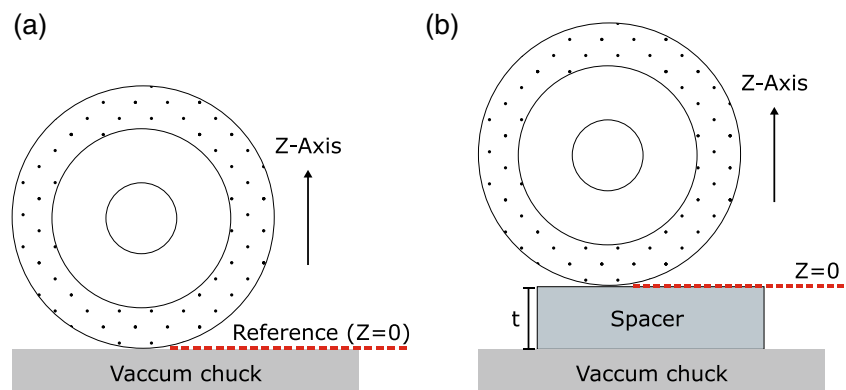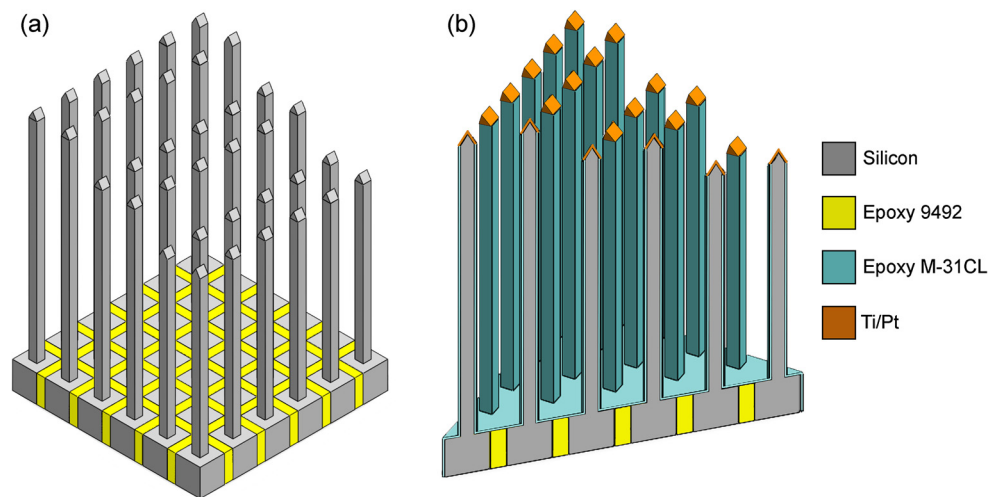
Fig. 3 **a** 3D MEA schematic after the blade dicing process to create the array design; **b** Transversal cut of the 3D final array showing the electrical insulation, encapsulation, and transduction layers

Arrays are fabricated out of a [100] p-type boron-doped silicon wafer with 1.3 mΩ cm resistivity and a thickness of 4.5 mm. The boron doped p-type silicon shows low resistivity, resulting in a substrate with good electrical characteristics and also strong enough under compression (Young modulus of 130 GPa). Nevertheless, silicon is a brittle material and, because of that, during dicing, microcracks and chipping might be created within the wafer [23].

During cutting steps of silicon wafers, a total of four blades coated with diamonds were used. Each blade exhibit different grit size, thickness, exposure, and shape suitable for each fabrication step. Their specifications are shown in Table 1. The experimental dicing parameters for each fabrication step are summarized in Table 2.

2.3.1 Pads regions

Fabrication process starts by making a set of deep cuts on the backside of the silicon wafer to create squared pads regions with dimensions of $0.45 \times 0.45 \times 1.5$ mm^3. Pads regions represent the electrical contacts of each electrode in the probe. This dicing step is carried out by a NBC-ZB blade (Fig. 4a), capable of performing grooves 150 μm wide and 1.5 mm deep (Fig. 5a). The cuts are programmed to be 600 μm spaced (y-axis step of 600 μm) and a feed speed of 0.5 mm s^{-1}.

Table 1 Diamond blades specifications used in the probe fabrication

Blade	Grit size	Exposure (mm)	Thickness (μm)	Shape (°)
NBC-ZB	#2000	4.28	150	0
Z09	#2000	5.28	250	60
Z05	#360	6.28	300	0
B1E8	#320	5.28	400	60

The silicon wafer surface is placed 4.5 mm above chuck surface, so Z-axis limit of 2 mm is exceeded. Thereby, a 3 mm-thick spacer is used for the calibration of Z-axis value. Since 1.5 mm-deep cuts are performed, Z-axis level is programmed to be 0.

Pads grooves are then filled with a non-conductive epoxy resin (Loctite® Hysol 9492), in order to electrically isolate each electrode from its neighbors. Epoxy excess is removed through grinding and polishing. After cutting electrode shafts, epoxy resin is used to hold all shafts in a single structure.

2.3.2 Staircase

The next fabrication step includes dicing the wafer upper side, in order to produce three steps with different heights. This is accomplished by multiple closely-spaced dicing cuts, so all the silicon between cuts is removed. This is ensured by a Y-axis step of 150 μm, which corresponds to the blade width. Each set of closely-spaced cuts produces a step that is 0.5 mm shorter than the previous one (Fig. 5b). Thus, the set of cuts for higher shafts is performed at the wafer surface, followed by a set of cuts 0.5 mm deeper and so on.

Just like the previous step, wafer surface is 4.5 mm above chuck surface, so Z-axis limit of 2 mm is exceeded. A 3 mm-thick spacer is used for the calibration of Z-axis value. Z-axis level of 1 mm is used to cut the middle step, while 0.5 mm is used for the lower step. Cut speed of 0.5 mm s^{-1} was used in this fabrication step.

2.3.3 Shafts

Fabrication of shafts represents the deepest cuts on entire fabrication process, reaching 4 mm-deep cuts. As the

Table 2 Experimental dicing parameters

Parameter	Fabrication steps					
	Pads region	Staircase	Blunt shafts	Sharpened tips	Encapsulation	Individualization
Cut speed (mm s^{-1})	0.5	0.5	0.3	0.5	0.3	0.5
Blade type	NBC-ZB	NBC-ZB	NBC-ZB	Z09	Z05	B1E8
Z-axis calibration (mm)	3	3	[a]0	3	0	0
[b]Z-axis level (mm)	0	1.5;1;0.5	0.5	1.25;0.75;0.25	0.565	0.05
Y-axis steps (mm)	0.6	0.15	[0.3,0.15]	[0.25,0.35]	[0.54,0.06]	4

[a]Chuck surface. [b]Z-axis step has a 2 mm limit. *Square brackets* represent a set of sequential Y steps, which are repeated during the cut.

2 mm limit is not exceeded, a standard Z-axis calibration is performed. Because of final pads' width, Z-axis level is set to 0.5 mm. NBC-ZB blade is used to this stage. With an exposure value of 4.28 mm (see Table 1), this blades is able to dice 4 mm-deep grooves.

Fig. 4 Photograph of the **a** NBC-ZB (DISCO NBC-ZB 2050 58 × 0.15 × 40), **b** Z09 (DISCO Z09 SD2000 Y1 120 60 × 0.25A3 × 40 × 60E V), **c** Z05 (DISCO Z05 SD360 D1 90 A8880 62 × 0.3A3 × 40), and **d** B1E8 (DISCO B1E801 SD320N50M42 60 × 0.4 × 40 × 60°) diamond blades. Zoom images were performed with a Leica M80^{TM} stereo microscope. The *small dots* seen over the blades (especially on B1E8 blade) are diamond grits
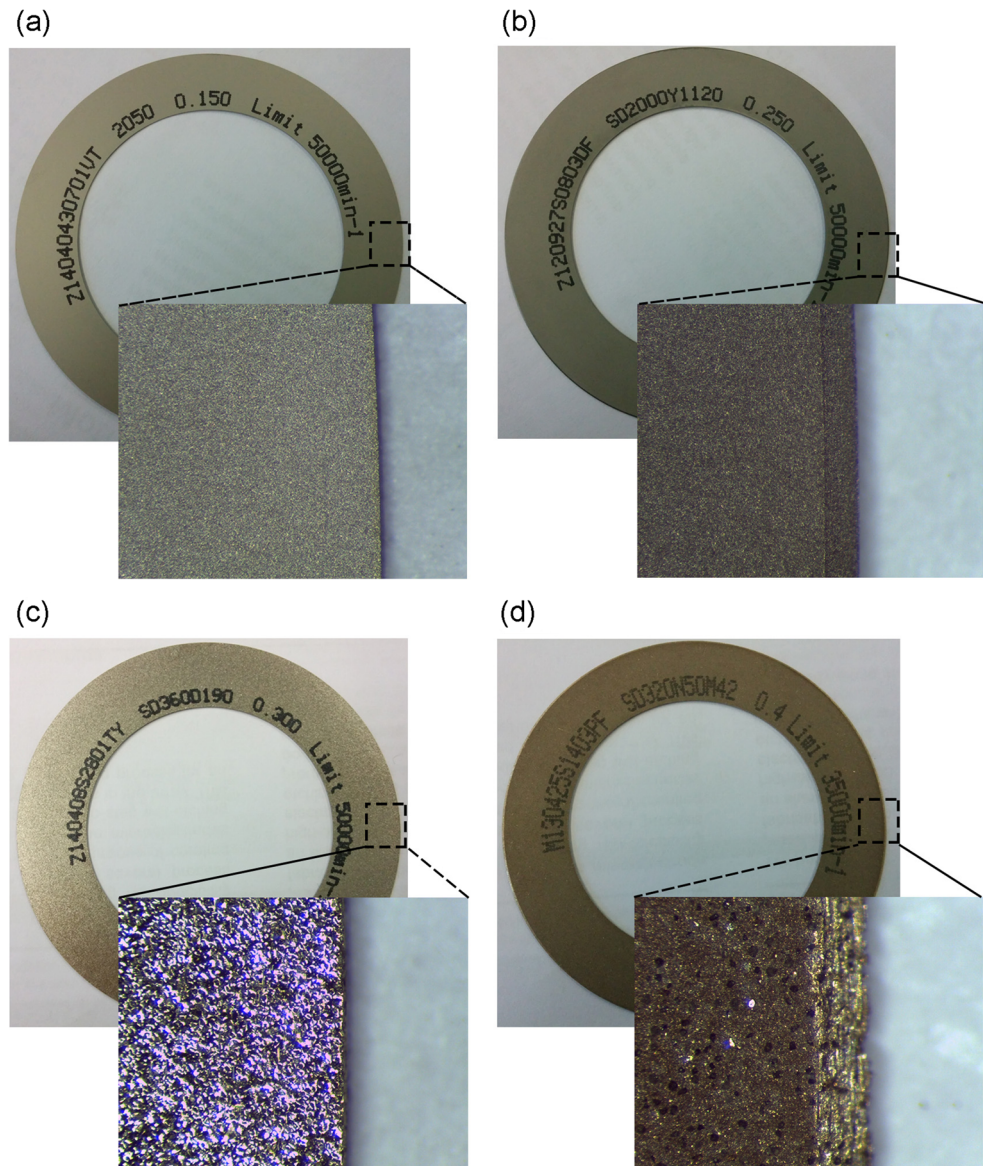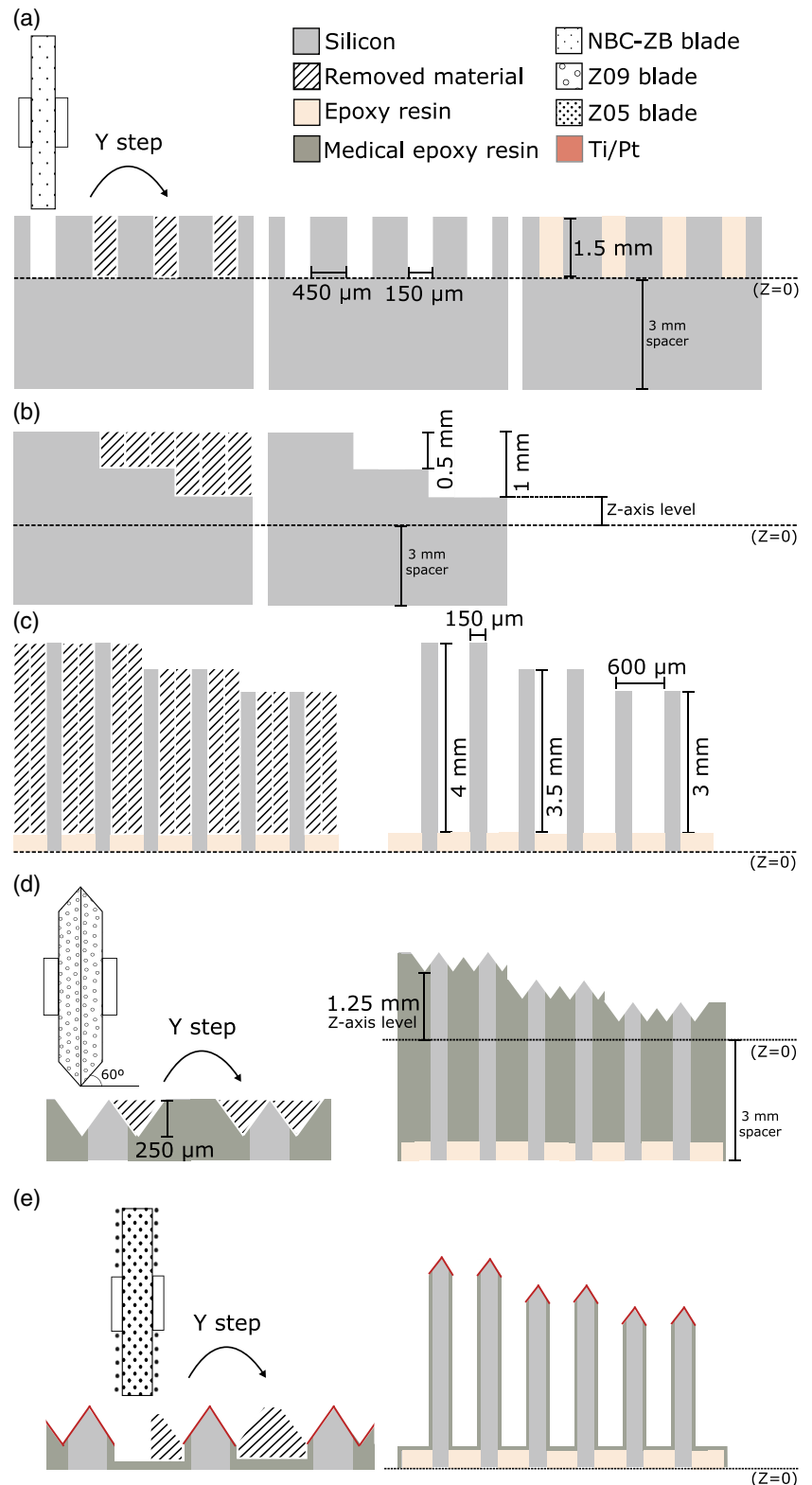
Fig. 5 **a** Dicing pads regions; **b** Saircase produced by closely-spaced cuts; **c** Blunt shafts with different lengths. These cutting steps used the NBC-ZB blade with a flat profile. **d** Sharpened tips dicing using the V-shape Z09 blade. **e** Medical epoxy excess removal by the Z05 blade. The illustration is not to scale

Cutting program consisted on two different *y*-axis steps: the first is 300 *μ*m and the second 150 *μ*m. The first step determines the thickness of the pillar, while the second determines the empty space between pillars. These two steps are repeated until the upper side of the silicon substrate is completely diced. Due to high blade exposure and fragility of shafts created in this step, cut speed was programmed to 0.3 mm s^{-1} (machine minimum feed speed).

Pads backside that were initially 1.5 mm deep are now reduced to a thickness of 0.5 mm, connected by a 0.15 mm wide layer of epoxy resin.

The result of this dicing step is thirty-six 0.15×0.15 mm^2 wide shafts with penetrating depths of 3, 3.5, and 4 mm (Fig. 4c). This technology also allows various combinations of shaft lengths (up to 4 mm), that could be suitable for other applications.

2.3.4 Sharp tips

Before sharpening the shafts tips, the array is completely covered with biocompatible resin (Loctite® M-31CL^{TM}). This medical epoxy serves as a selective mask to control the area where transduction layer will be deposited, since after dicing step only silicon material is exposed at the tips. Array filling is accomplished by placing it into a square mold filled with medical epoxy adhesive.

Sharpening process is performed in order to smooth electrodes implantation procedure into brain tissue. Since blunt shafts comprise different lengths, this step has to be completed once again at increasing depths with a Z-axis difference (index) of 0.5 mm between cuts. Z-axis calibration was performed with a 3 mm-thick spacer and 250 μm-deep cuts were programmed at different indexes (three different Z-axis levels). Therefore, sharpened shafts with different lengths are produced, as shown in Fig. 5d. This dicing step is accomplished by Z09 blade that makes a 60° angle with the surface (Fig. 4b). Cutting speed is increased to 0.5 mm s^{-1}.

Sharp tips must be aligned with shafts middle plane (half pillar width), which is accomplished using the microscope of the equipment. After the first cut, a 250 μm Y-axis step is made, which represents blade width. Relying only on these two cuts sharpening process is accomplished in one electrode. The second Y-axis step is 350 μm and determines the start of the next sharp tip. These Y-axis sets are repeated until shaft upper side is completely diced.

2.3.5 Encapsulation

At this point of fabrication, the array is completely filled with medical epoxy, with the exception of tips. Therefore, transduction layer is deposited, converting the silicon shafts into active electrodes for recording or stimulation. The transduction layer consists of 50 nm of titanium (adhesive layer) deposited using electron beam evaporation and 200 nm of a platinum layer deposited using DC sputtering.

The final dicing step consists on removing excesses of medical epoxy from inter-shafts spaces. For this step, Z05 blade (Fig. 4c) was used and due to its protruding diamond

grits, the saw grooves performed show an approximate width of 360 μm (superior to blade width). A standard Z-axis calibration is performed. Due to high volume of epoxy to be removed, the cutting speed was 0.3 mm s^{-1}.

Cutting program also comprises two different y-axis steps: the first is 540 μm and the second 60 μm. The first step performs 360 μm wide grooves between shafts and determines the thickness of the encapsulated pillar (180 μm), while the second removes the remaining epoxy. After this step each, shafts comprise epoxy encapsulation layers of 15 μm all around it (Fig. 5e). These two steps are repeated until wafer upper side is completely diced. Due to low thickness of encapsulation layer, while setting the Z-axis level value, it must be taken into account the thickness of the dicing tape ($\simeq$ 50 μm). Z-axis level is then programmed to be 565 μm. The result is thirty-six 180×180 μm^2 wide shafts with different penetrating depths and active tips.

2.3.6 Individualization

Singularization of the each electrode from the wafer is accomplished by B1E8 blade (Fig. 4d), since it exhibits enough exposure to perform 4.5 mm-deep cuts. The cut speed is 0.5 mm s^{-1} and a standard Z-axis calibration is performed. In order to prevent chuck damage, Z-axis level is set to 50 μm (dicing tape thickness).

3 Results and Discussion

Results of each fabrication step are shown in Fig. 6 with multiple views of the diced silicon wafer. For clarity of fabrication steps, it will only be exhibited dicing results of an array sample. All photos and measurements were performed with a Leica M80^{TM} stereo microscope and Leica LAS^{TM} software.

The results of pads regions dicing are shown in Fig. 6a, as well as groove filling with epoxy resin. Initially, pads regions were $0.45 \times 0.45 \pm 0.013$ mm^2 wide and 1.5 ± 0.027 mm deep. Upper side silicon staircase can been seen in the photo of the array in Fig. 6b. This closely-cuts stage introduced small rails in the wafer surface (direction of the blade passage), which are visible in the figure. Figure 6c shows the result of shafts formation diced in one direction, producing 150 μm wide walls with different lengths. The staircase and the cut rails are also possible to be seen from top view. After a new set of cuts made perpendicularly, it is obtained a matrix of 600 μm spaced blunts shafts (Fig. 6d). The shafts created are 4 ± 0.017 mm, 3.5 ± 0.009 mm, and 3 ± 0.014 mm deep, and 0.15 ± 0.005 mm wide. At this stage, the final contact pads are 0.5 ± 0.043 mm thick. Both distances between shafts and their shape were measured
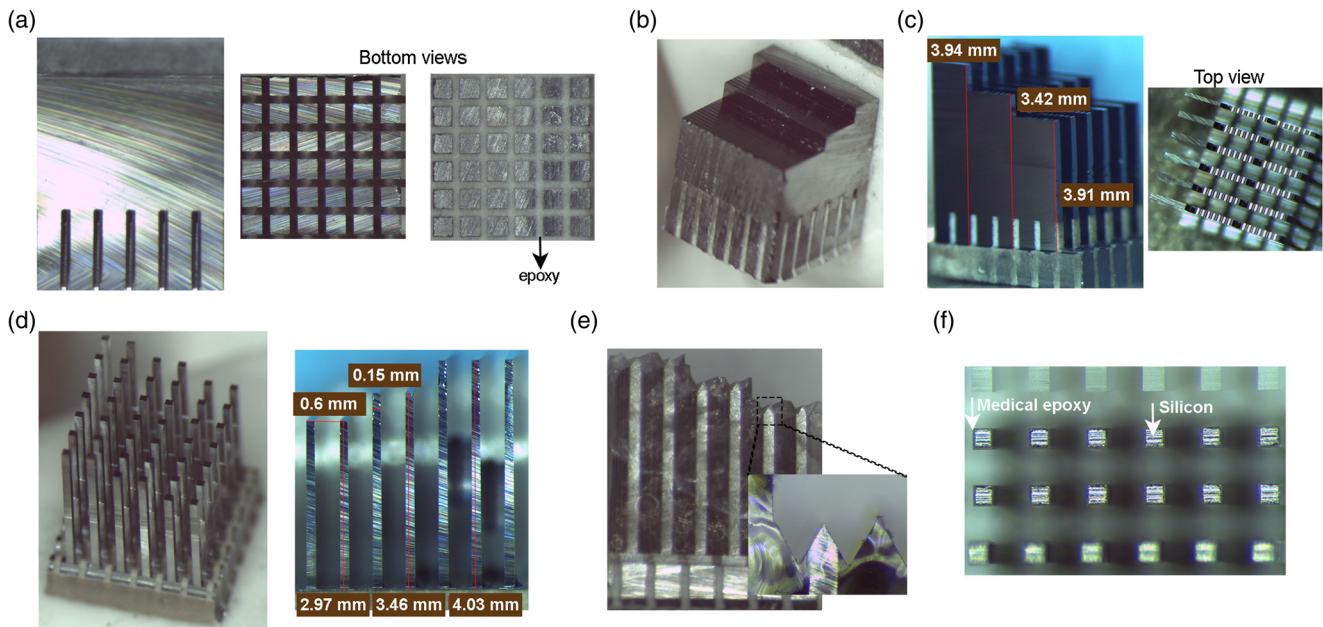
Fig. 6 Fabrication process photos. **a** Cross-section and bottom views of the diced pads regions, with and without epoxy resin; **b** staircase; **c** array after a first set of cut in the one direction, with measurements of the shafts' final length. In top view, the closely-spaced cuts are clearly visible. **d** Blunt shafts with different lengths and spaced 600 μm apart; **e** Sharpened tips dicing after encapsulation; **f** cross-section of the final shafts with a 15-μm wide encapsulation layer around it

using the optical microscope, with an error of ± 2 nm. Rectangular shaft shape was obtained by performing measurements ($n = 10$) in three different regions along shaft body (bottom, middle, and top). Results show maximum shafts width variation of 1.82 % (mean = 1.26 %, standard deviation = 0.86 %).

The first three fabrication steps were successfully accomplished by NBC-ZB blades. Both sides of these blades contain diamonds grits that minimize surface chipping, slanted cuts, and improve cutting quality. Compared to others blades, NBC-ZB show fine grit size, required for high-quality processing, such as deep and narrow grooves [15]. Although longer blade exposure is associated to larger chipping [18], chipping free cuts can be seen at all three fabrication stages (Fig. 6a–d).

NBC-ZB blades are recommended by the supplier to cut various types of ceramics and silicon with a maximum blade exposure ratio of 20:1, i.e, the cut depth should not exceed 20 times the groove width. Improper combination of thin blades with high blade exposure may cause blade instability during cut and ultimately result in blade breaking [24]. In NBC-ZB particular case, for a 150 μm-thick blade, a maximum 3 mm-deep cuts are recommended. Therefore, in order to compensate excess in the depth cut, the silicon wafer processing required very slow cut speeds (0.5 mm s^{-1} for pads regions and staircase and 0.3 mm s^{-1} for shafts formation), in contrast with high speed rates (70 mm s^{-1}) normally used in the semiconductor industry [21]. During shaft formation step,

attempts to increase cut speed resulted in shafts breaking and silicon microcracks, as shown in Fig. 7. Yet, blade integrity was maintained. Gatzen et al. [21] and Kim et al. [25] studied the effect of feed rate on dicing grooves quality. Both concluded that while dicing silicon wafers, wafer chipping increases with feed rate. Further in this discussion will be presented a study assessing the effect of increasing cut speed on surface roughness of silicon and epoxy substrates.

At this point of fabrication array density is settled. This feature is determined by the minimum blade's saw streets, so ultra-thin blades (thickness of 15–60 μm) should have been the proper choice. Nevertheless, the used of ultra-thin blades would result in even more demanding blade exposure ratio [26] and 4 mm-deep cuts in the wafer processing would be hindered.

The results of arrays filling with encapsulation material and tip formation are shown in Fig. 6e. Initially, shafts are entirely encapsulated by medical epoxy layer, but after dicing sharp tips, they become suitable for depositing transduction layers. The tip profile is determined by V-shaped grooves that bevelled Z09 blades are capable of making. Each cut is able to perform V-shaped grooves. Z09 blades used in this stage are also recommended by the supplier to cut various types of ceramics and silicon wafers. Scanning electron microscope (SEM) images are provided in Fig. 8 to show cut quality after tips dicing. The final tips show lengths of 0.15 ± 0.006 mm and tip radius of 2.41 μm. The tip measurement was performed in a FEI Nova NanoSem^{TM} 200 machine.
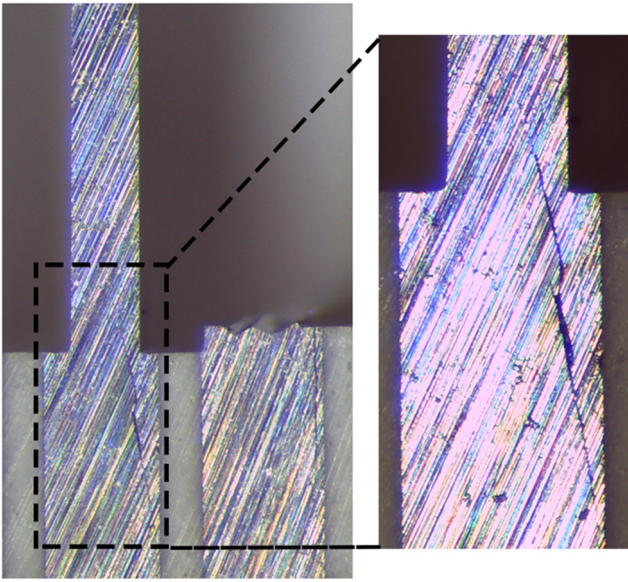
Fig. 7 Microcracks on silicon shafts resulting of high speed cuts

Although fabrication of tips does not require deep cuts into the wafer, low cut speeds are employed at this step, so the fabrication of high-quality tips is ensured. This speed value is consistent with those reported by Baranski et al. [27]. In his study, bevelled blades were employed to produce 45° slanted mounts in a glass substrate at 0.2 mm s^{-1}. Still the slanted surfaces reported are only 400 μm deep.

Final fabrication stage consisted on the removal of exceeding medical epoxy, which was accomplished by Z05 blade. These blades are also recommended by the supplier to cut various semiconductor packages such as ceramics, glass, and epoxies. The result is a 15 $\pm$ 3.6 μm encapsulation layer around shafts. A 6×6 matrix of 180×180 μm^2 wide electrodes with different penetrating depths spacing each electrode by 600 μm was successfully produced.

Although NBC-ZB blade seemed suitable to performed this dicing step, since it shows enough exposure, it is not recommended to saw epoxies. In fact, attempts to use NBC-ZB blade to perform this fabrication stage were made and saw grooves deeper than 1 mm resulted in blade breakage. B1E8 is also too thick to perform this stage, since it exhibits large diamond grits and cut quality of the dicing process would be diminished.

After several sets of cuts, all blades maintained their functionality. Quality of cuts was assessed by measuring wafer roughness along fabrication conditions. Roughness measurements were carried out by a profilometer Dektak model 150 with a 12.5 μm radio stylus using a force of 3 mg. For each sawing condition, roughness of three samples and three different areas on each sample were measured. Uncut silicon wafers showed an average roughness of 2.56 $\pm$ 0.12 nm. While creating the staircase on silicon, average surface roughness increased to 176.48 $\pm$ 15.63 nm, due to the rails created by NBC-ZB closely-spaced cuts. The rails created by these cuts can be seen in Fig. 9b. The pattern repeated every 150 μm corresponds to blade thickness. The steps show an average height of 501.84 $\pm$ 0.93 μm (Fig. 9a), as expected. The steps geometry appears slightly slanted due to the conical geometry of the profilometer stylus that cannot accurately measure long vertical steps. Shaft wall roughness was also measured with a value of 87.16 $\pm$ 12.49 nm. The shafts walls show an average roughness lower than silicon surface, because they result from a single lateral passage of the blade. Tips profile was also obtained (Fig. 9c), measuring a height of 164.43 $\pm$ 1.87 μm and average surface roughness of 69.94 $\pm$ 8.13 nm. Tips roughness can be visually seen in Fig. 8b, where the passage of the blade diamonds are easily identified.

As discussed before, attempts to increase cuts speed resulted in shafts breakage due to performed high-aspect ratio saw grooves. Nevertheless, the machining parameter that mostly influences surface roughness is the blade grit size. In order to study the influence of this parameter on surface roughness, cuts were made on silicon substrates with NBZ-ZB blades (fine grit size—see Table 1) and in

Fig. 8 SEM photos of the (**a**) array's sharp shafts and (**b**) radius tip
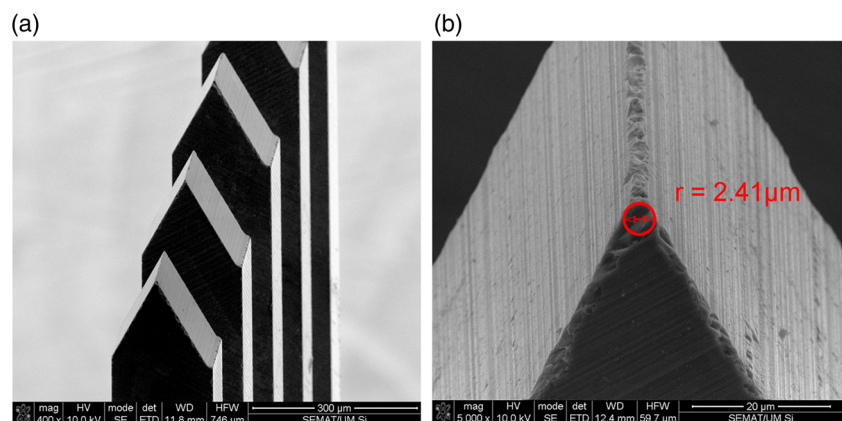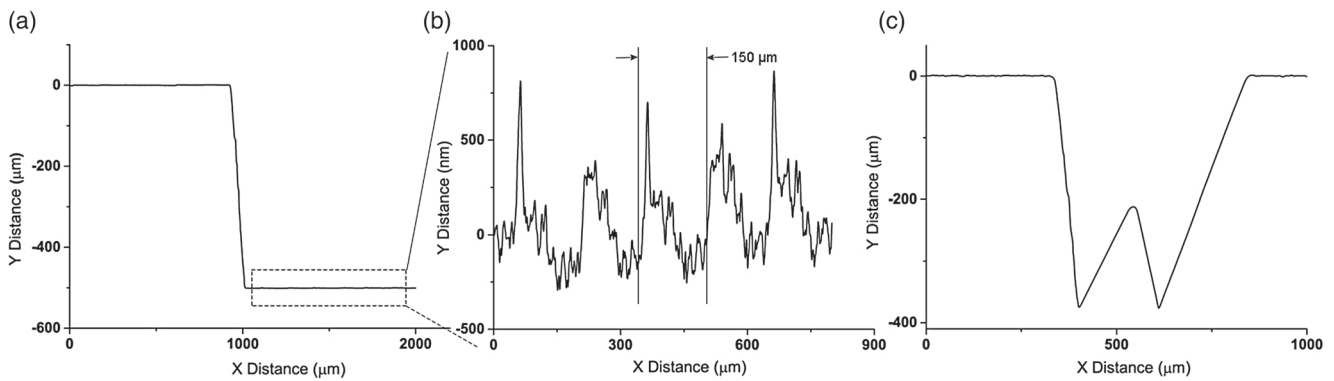
Fig. 9 Profilometer results. **a** Staircase step and **b** cut rails. **c** Tip profile

epoxy substrates with Z05 blades (thicker diamond grits) at different cut speeds.

Figure 10 shows roughness variation both in silicon and epoxy substrates for different cut speeds. Measurements were made in a total of three samples per cut speed for each substrate ($n = 6$), in two different areas on each sample. The cut speed ranges from the minimum speed of the equipment (0.3 mm s^{-1}) to 3 mm s^{-1}, which is a high cut speed to produce such a complex device. As expected, the roughness on silicon surfaces tends to increase with the increment in cut speed. Similarly, roughness on epoxy surfaces has increased from 0.3 mm s^{-1} to 0.5 mm s^{-1}. In fact, it was observed areas with cracks within the sample surface, which could explain the increasing of the roughness magnitude. However, it is shown the decrease in epoxy roughness for cut speeds of 1 and 1.5 mm s^{-1} comparing to 0.5 mm s^{-1}. This low roughness can be the result of measurements performed in areas not cracked. On the other hand, it is possible to observe a significant increase
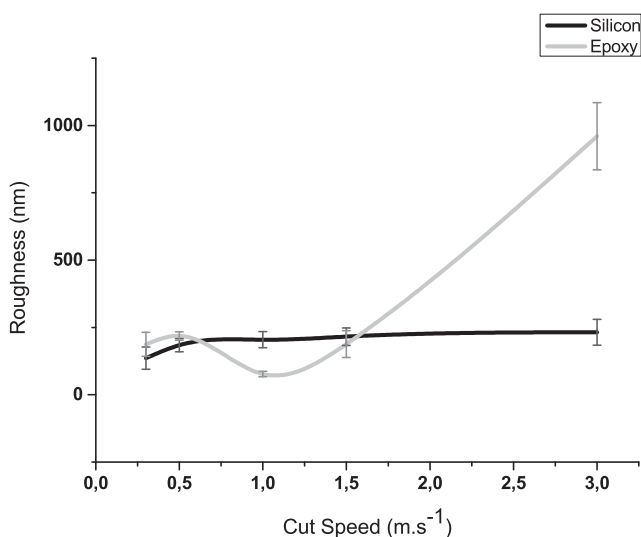
in epoxy roughness at 3 mm s^{-1} due to the high number of areas with cracks on the samples. In overall, it is concluded that the best results are obtained at lower cut speeds both for silicon and especially for epoxy substrate, which is the layer interfacing with neural tissue. Thus, for the lowest cut speed, silicon and epoxy substrates achieved an average surface roughness of 136.3 and 187.2 nm, respectively. Table 3 shows roughness values for each cut speed and substrate.

The exclusively use of a blade dicing process for the 3D array creation show some advantages. It is a standard microfabrication technology and it is attractive by its simplicity and cost-effectiveness. However, particles and ionic contamination could be a problem in the final quality of the diced substrates. In fact, as dicing blades cut through the wafer, particles are created. Most of these particles are suspended in water and then carried away by the deionized water jet being showered on the wafer. The particles that remain on the wafer are easily washed away with the machine nitrogen spray gun.

Overall, due to the physical contact between dicing blades and wafers surface, chipping and cracking are hard to eliminate. The effect of chipping and cracking may be aggravated when dicing thicker wafers, since they require longer blade exposure to saw through [28]. This effect can be minimized by choosing proper blades and dicing parameters, such as low feed speed [24, 25]. Results suggest all fabrication steps were free of chipping and cracks. To

Fig. 10 Roughness variation along silicon and epoxy surfaces for different cut speeds

Table 3 Roughness results for silicon and epoxy substrates

Cut speed (mm s^{-1})	Silicon (nm)	Epoxy (nm)
0.3	136.3 ± 41.2	187.2 ± 44.9
0.5	184 ± 24.1	218.1 ± 15.6
1	204.4 ± 29.8	77 ± 10.1
1.5	215.9 ± 32.5	188.3 ± 50
3	232.2 ± 48.1	960 ± 124.7

accomplish this, low cutting speeds were necessary, which implied higher fabrication time.

Other techniques for dicing silicon wafers have been used, such as laser dicing [24] and stealth dicing [14]. Both these methods rely on laser processes. Stealth dicing works by stress-cutting the substrate from the "inside", being fundamentally different from laser dicing that cuts from "outside". While they eliminate physical contact with the wafer and consequently reduce chipping process, its application is reserved to thin wafers ($< 100 \mu$m) [14]. Therefore, dicing thick wafers would have to involve a combination of laser and mechanical saw [24]. Due to the possibility of high-speed and quality cuts, laser methods could be used in case of creation several μm deep groove saws. Cheung et al. [29] have shown high yield in thin wafers processing during mechanical dicing by improving dicing parameters, without having to resort to higher cost laser dicing. Fan et al. [28] also proposed a low-cost method for dicing silicon wafers using a craft cutter. Whereas the employed cut speed is high (40 mm s^{-1}), it also uses diamond blades and cut depth is limited to 7.5 μm.

By employing an entirely mechanically cutting technology, this study demonstrated a technology capable of producing high-accuracy and complex 3D microstructures. These characteristics have already been discussed by Cheng et al. [17], which show some advantages of the mechanical micro machining over standard MEMS-based processes, such as wider materials choice, high accuracy, and capability of producing complex 3D geometry microparts. In this paper, it were addressed all the process parameters to ensure predictability, repeatability, and productivity of devices that include manufacturing processes of microparts.

4 Conclusion

The fabrication process of a 3D complex MEA is described, relying exclusively on a standard micromachining technology: conventional blade dicing. The proposed method was able to overcome the limitations imposed by dicing machines and fabrication challenges, by introducing new and simple method for Z-axis calibration. Moreover, this method broadens dicing opportunities for thick wafers on several applications.

The fabrication process is mainly characterized by its simplicity and reproducibility. The effect of several cut speeds on MEA roughness was studied and it was found that higher speeds suggest increased roughness on substrates. Thus, together with the fact that several deep cuts are performed, feed speed of the entire fabrication process was kept very low (0.5 and 0.3 mm s^{-1}), which may be time-consuming. Analysis and decision on the proper blade is also mandatory, changing with the demands of each fabrication step. High exposure blades are used to accomplish deep saw grooves and bevelled blades for the sharp tips. The overall result is a high-precision and quality 3D neural probe comprising 36 individually addressable electrodes (with a 3, 3.5, and 4 mm length). Nevertheless, there is still much room for improvement; it should be possible to increase arrays density, for example, by using thinner blades, and also reduce shafts width, improving electrodes aspect-ratio.

References

1. Ruther P, Herwik S, Kisban S, Seidl K, Oliver P (2010) Recent progress in neural probes using silicon MEMS technology. IEEJ Trans Electr Electron Eng 2010 (5):505–515
2. Seidl K, Herwik S, Torfs T, Neves H, Paul O, Ruther P (2011) CMOS-based high-density silicon microprobe arrays for electronic depth control in intracortical neural recording. J Microelectromech Syst 20:1439–1448
3. Chang C, Chiou J (2010) Development of a three dimensional neural sensing device by a stacking method. Sensors 10:4238–4252
4. Gabran S, Salam M, Dian J, El-Hayek Y, Velazquez J, Genov R, Carlen P, Salama M, Mansour R (2014) 3-D flexible nano-textured high-density microelectrode arrays for high-performance neuromonitoring and neuro-stimulation. IEEE Trans Neural Syst Rehab Eng 22:1072–1082
5. Wang M, Maleki T, Ziaie B (2010) A self-assembled 3D microelectrode array. J Micromech Microeng 20:035013
6. Chavert G, et al. (2010) BioMEA^{TM}: a versatile high-density 3D microelectrode array system using integrated electronics. Biosens Bioelectron 25:1889–1896
7. Merriam M, Dehmel S, Srivannavit O, Shore S, Wise K (2011) A 3-D 160-site microelectrode array for cochlear nucleus mapping. IEEE Trans Biom Eng 58:397–403
8. Rakwal D, Heamawatanachai S, Tathireddy P, Solzbacher F, Bamberg E (2009) Fabrication of compliant high aspect ratio silicon microelectrode arrays using micro-wire electrical discharge machining. Microsyst Technol 15:789–797
9. Takeuchi S., Suzuki T., Mabuchi K., Fujita H. (2004) 3D flexible multichannel neural probe array. J Micromech Microeng 14:104–107
10. Campbell P, Jones K, Huber R, Horch K, Normann R (1991) A silicon-based, three-dimensional neural interface: manufacturing processes for an intracortical electrode array. IEEE Trans Biom Eng 38:758–768
11. Peixoto A, Goncalves S, Silva A, Dias N, Correia J (2013) Neural electrode array based on aluminum: fabrication an characterization. IEEE Sensors J 13:3319–3324
12. Goncalves S, Peixoto A, Silva A, Correia J (2013) High.aspect ratio microelectrodes array with different penetrating lengthfor neural applications, Micromechanics and Microsystems Europe Conference, Espoo, Finland
13. Arif M, Rahman M, San W (2012) A state-of-the-art review of ductile cutting of silicon wafers for semiconductor and microelectronics industries. Int J Adv Manuf Technol 63:481–504
14. Kumagai M, Uchiyama N, Ohmura E, Sugiura R, Atsumi K, Fukumitsu K (2007) Advanced dicing technology for semiconductor

wafer–stealth dicing. IEEE Trans Semiconductor Manufacturing 20:259–265

15. Zhou H, Qiu S, Huo Y, Zhang N (2013) High-speed dicing of silicon wafers conducted using ultrathin blades. Int J Adv Manuf Technol 66:947–953

16. Jiun H, Ahmad I, Jalar A, Omar G (2006) Effect of laminated wafer toward dicing process and alternative double pass sawing method to reduce chipping. 2006 IEEE Trans Electronics Packaging Manufacturing 29:17–24

17. Cheng K, Huo D (2013) Micro cutting: fundamentals and applications. John Wiley & Sons Ltd, Chichester

18. Wang Z, Wang J, Lee S, Yao S, Han R, Su Y (2007) 300-mm low-k wafer dicing saw development. IEEE Trans Electronics Packaging Manufacturing 30:313–319

19. Luo S, Wang Z (2008) Studies of chipping mechanisms for dicing silicon wafers. Int J Adv Manuf Technol 35:1206–1218

20. Rao R, Kalyankar V (2014) Optimization of modern machining processes using advanced optimization techniques: a review. Int J Adv Manuf Technol 73:1159–1188

21. Gatzen H (2001) Dicing challenges in microelectronics and micro electro-mechanical systems (MEMS). Microsyst Technol 7:151–154

22. Chen S, Tsai C, Wu E, Shih I, Chen Y (2006) Study on the effects of wafer thinning and dicing on chip strength. IEEE Trans Advanced Packaging 29:149–157

23. Bidiville A, Wasmer K, Michler J, Nasch P, Van der Meer M, Ballif C (2010) Mechanisms of wafer sawing and impact on wafer properties. Prog Photovolt Res Appl 18:563–572

24. Amri M, Liew D, Harun F (2010) Chipping free process for combination of narrow saw street (60 μm) and thick wafer (600 μm) sawing process, IEEE/CPMT Int. Electronic Manufacturing Technology Symposium

25. Kim S, Lee E, Kim N, Jeong H (2007) Machining characteristics on the ultra-precision dicing of silicon wafer. Int J Adv Manuf Technol 33:662–667

26. Ganesh V, Lee C (2006) Overview and emerging challenges in mechanical dicing of silicon wafers, IEEE Electronics Packaging Technology Conference (Singapore, 6–8 December)

27. Baranski M, Bargiel S, Passily N, Guichardaz B, Herth E, Gorecki C, Jia C, Frömel J, Wiemer M (2014) Wafer-level fabrication of microcube-typed beam-splitters by saw-dicing of glass substrate. IEEE Photon Technol Lett 26:100–103

28. Fan Y, Arevalo A, Li H, Foulds I (2014) Low-cost silicon wafer dicing using a craft cutter. Microsyst Technol. doi:10.1007/s00542-014-2198-4

29. Cheung A (2005) Dicing advanced materials for microelectronics, proceedings of IEEE International Symposium on Advanced Packaging Materials: Processes, Properties and Interfaces (Irvine, CA, 16–18 March)